Laminar Separation Bubble Characteristics on an Airfoil at Low Reynolds Numbers

M. M. O'Meara* and T. J. Mueller†
University of Notre Dame, Notre Dame, Indiana

An experimental investigation was conducted in order to document the structure and behavior of laminar separation bubbles at low Reynolds numbers. Data of this type are necessary if the currently insufficient analytical and numerical models are to be improved. The laminar separation bubble that forms on a NACA 66_3-018 airfoil model was surveyed at chord Reynolds numbers of 50,000–200,000 at angles of attack of 8–12 deg. The effects of the various testing conditions on the separation bubble were isolated and the data were analyzed in relation to existing separation bubble correlations in order to test their low Reynolds number applicability. This analysis indicated that the chord Reynolds number and the disturbance environment strongly influence the experimental pressure distributions. These effects must be included in any analytic prediction technique applied to the low Reynolds number flight regime.

Nomenclature

B = proportionality constant relating the momentum thickness Reynolds number at separation to the tangent of the separation angle
C = airfoil chord, mm (in.)
C_P = pressure coefficient $(P_i - P_{fs})/Q_{fs}$
H_B = height (thickness) of the region of separated flow at a given station, mm (in.)
H_T = height of transition = height of the maximum turbulence intensity point at transition, mm (in.)
H_{12} = boundary-layer shape factor, δ_1/δ_2
H_{32} = boundary-layer shape factor, δ_3/δ_2
K = proportionality constant suggested by Horton
l_B = surface arc length of entire separation bubble, mm (in.)
l_1 = surface arc length of laminar portion of bubble, mm (in.)
l_2 = surface arc length of turbulent portion of bubble, mm (in.)
P = static pressure, mm (in.) of Hg or H_2O
Q = dynamic pressure, $\rho U_{fs}^2/2$, Pa (lb/ft^2)
R = approximate location of turbulent reattachment
R_c = Reynolds number based on freestream velocity and chord length, $U_{fs}C\rho/\mu$
R_{li} = Reynolds number based on external velocity at separation and reference length l_i, $U_S l_i \rho/\mu$
$(R_S)_i$ = Reynolds number based on external velocity at separation and surface arc length from stagnation point to point i, $U_S S_i \rho/\mu$
R_{δ_i} = Reynolds number based on local external velocity and local integrated boundary-layer thickness δ_i, $U_S \delta_i \rho/\mu$
S = surface arc length coordinate
S = approximate location of laminar separation
S' = approximate location of turbulent separation
S/C = nondimensional distance along airfoil surface
T = approximate location of flow transition
U = mean velocity
X = axis along airfoil chord
X/C = nondimensional distance along chord
α = airfoil angle of attack
α_T = turbulent spreading angle
γ = separation angle
δ = approximate boundary-layer thickness
δ_1 = boundary-layer displacement thickness, mm (in.), $\int_0^\delta (1 - U/U_{ext})dH$
δ_2 = boundary-layer momentum thickness, mm (in.), $\int_0^\delta U/U_{ext}[(1 - U/U_{ext})]dH$
δ_3 = boundary-layer energy thickness, mm (in.), $\int_0^\delta U/U_{ext}[1 - (U/U_{ext})^2]dH$
μ = absolute air viscosity, kg/m·s(slug/ft·s)
ρ = air density, kg/m^3 (slug/ft^3)

Subscripts

B = separation bubble
ext = local conditions at edge of boundary layer
fs = freestream conditions
i = pressure tap i (indicates arbitrary reference quantity)
R = conditions at turbulent reattachment
S = conditions at laminar separation
S' = conditions at turbulent separation
T = conditions at free shear layer transition

Introduction

BEFORE the design or analysis of airfoils operating in the low Reynolds number flight regime can be improved, a better understanding of the associated flow phenomena must be achieved. For low Reynolds number incompressible flows, careful management of the airfoil boundary layer is required to alleviate the likely deterioration in airfoil performance. The major concerns at these conditions involve the large regions of separated flow that can occur over the airfoil. In particular, the various flow phenomena involved in the formation of a laminar separation bubble are of interest, since they play an important role in the development of the boundary layer. These phenomena are collectively illustrated in Fig. 1.

A laminar separation bubble is formed when the previously attached laminar boundary layer encounters an adverse pressure gradient of sufficient magnitude to cause the flow to separate. Downstream of the point of separation, denoted by S in Fig. 1, the flow can be roughly divided into two main regions.[1] The first region is bounded by the mean dividing

Received March 24, 1986; presented as Paper 86-1065 at the AIAA/ASME Fourth Fluid Mechanics, Plasma Dyanmics and Lasers Conference, Atlanta, GA, May 12-14, 1986; revision received Dec. 8, 1986.

*Graduate Research Assistant, Department of Aerospace and Mechanical Engineering (presently Lieutenant, U.S. Air Force Wright-Patterson AFB, OH).

†Professor, Department of Aerospace and Mechanical Engineering. Associate Fellow AIAA.

streamline ST′R and the airfoil surface. The mean dividing streamline is generally regarded as the collection of points across each velocity profile at which the integrated mass flow is zero. This first region represents the relatively slow recirculatory flow forming the bubble.

The second region of flow consists of the free shear layer contained between the outer edge of the boundary layer S″T″R″ and the dividing streamline. This separated shear layer undergoes transition at a location denoted by T due to disturbance amplification occurring in the unstable laminar layer. Momentum transfer due to turbulent mixing eventually eliminates the reverse flow near the wall and the flow reattaches at point R. This process of separation, transition, and reattachment results in a laminar separation bubble that has a predominate effect on the entire airfoil flowfield; therefore, it must be fully documented before low Reynolds number aerodynamics can be fully understood.

In order to provide such documentation, a detailed experimental study was conducted of the laminar separation bubbles that form near the leading edge of an NACA 66_3-018 airfoil. The data acquisition phase of the investigation was focused on quantifying the various separation bubble parameters shown schematically in Fig. 2. This figure illustrates the simplified bubble model suggested by Eppler.[2] Static pressure, hot-wire anemometry, and flow visualization data were acquired at Reynolds numbers of 50,000–200,000 at angles of attack of 8–12 deg. Once acquired, the data were used to evaluate the low Reynolds number applicability of several existing separation bubble models.[2] This paper will address some of the important results of this analysis.

Apparatus and Procedure

The low-speed wind tunnel used in this investigation was an indraft type with atmospheric exhaust. The important features and dimensions of the wind tunnel are illustrated in Fig. 3. In order to achieve certain testing conditions, the basic tunnel configuration was slightly altered through the introduction of flow restricting devices. These devices consisted of a wooden frame packed with plastic drinking straws. The flow restrictors, when used, were clamped securely between the test section and the diffuser.

The effect of introducing one or two flow restrictors was to change the overall disturbance environment in the tunnel. When inserted, the flow restrictors caused an increase in both the acoustic and turbulence levels in the test section. These increases were due primarily to the higher fan speeds required to compensate for the pressure drop across the flow-restricting devices.[3] The combined effect of introducing the flow restrictions was utilized to study the sensitivity of the separation bubble flowfield to changes in the freestream disturbance environment. No attempt was made to isolate the effects of increased acoustic levels from increases in freestream turbulence.[3,4] Typical freestream turbulence intensities are presented in Table 1 and nominal levels of acoustic disturbances are given in Ref. 3.

All of the wind-tunnel tests were performed using two NACA 66_3-018 airfoil models mounted in a $610\times610\times1810$ mm long test section. Both of these models had a chord of 250 mm and a span of 410 mm. The first model was made of smooth epoxy and was used for all of the hot-wire anemometry experiments. The second model, also made of epoxy, was equipped with 93 static pressure taps and used to obtain the airfoil pressure distributions. This model was constructed with 46 upper surface taps, 46 lower surface taps, and 1 leading-edge tap. For testing, the airfoil models were mounted horizontally between large end plates in order to produce a two-dimensional geometry.

Static pressure distributions were obtained using the pressure tap model and a series of pressure transducers and switching mechanisms. The airfoil pressure taps were connected through Tygon tubing to two Scanivalve main body devices. These devices were designed to transmit the pressures to electronic manometers (Setra Systems) and to switch the pressure passage sequentially from tap to tap. The analog-to-digital and digital-to-analog capabilities of an appropriately configured Digital Equipment Corporation PDP 11/23 minicomputer were used to sample the analog output of the manometers and to automatically step through a complete series of pressure taps. Freestream dynamic pressures were measured with a standard pitot-static tube placed upstream of the model.

The boundary layer over the airfoil was surveyed in a two-step process using a Thermal Systems Inc. hot-wire

Table 1 Typical freestream tubulence intensities, %

	No. of flow restrictors		
R_c	0	1	2
200,000	0.160	—	—
160,000	0.129	—	—
140,000	0.108	0.167	0.296
100,000	—	0.147	—
80,000	—	0.134	—
50,000	—	0.125	0.220

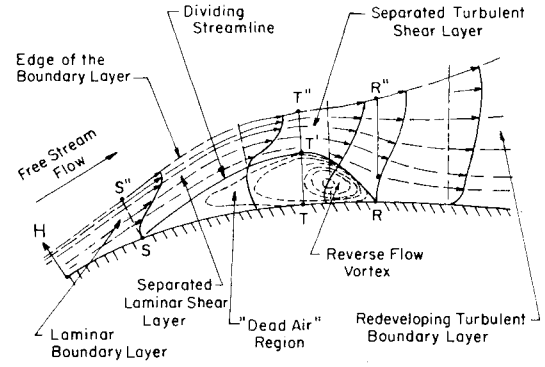

Fig. 1 Section view of laminar separation bubble (from Ref. 8).

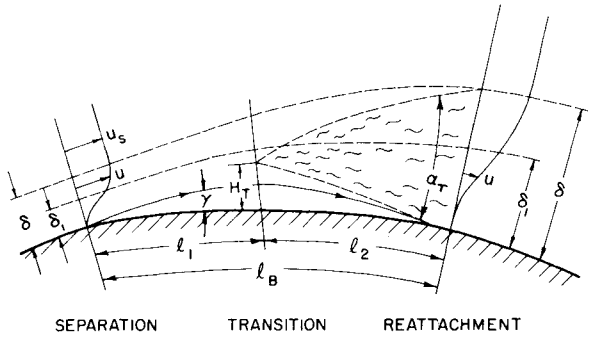

Fig. 2 Two-dimensional separation bubble model suggested by Eppler (Ref. 2).

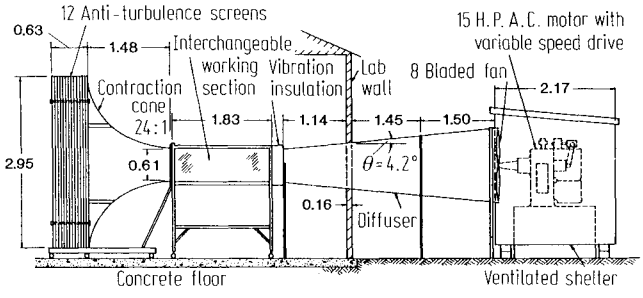

Fig. 3 Notre Dame Aerospace Laboratory wind tunnel (dimensions in meters).

anemometry system. The anemometer unit (model 1050) was operated in the constant-temperature mode with a DISA type 55P15 single-wire boundary-layer probe that was calibrated before each test using specially designed software. The first phase of the hot-wire anemometry experiments involved measuring the mean and fluctuating velocity components of the boundary layer at 20–24 stations along the airfoil's upper surface. The locations of these stations varied depending on the size and position of the separation bubble. Data were acquired at 51 points in each profile with each point representing an ensemble of 500 samples. The second phase of hot-wire testing involved the acquisition of energy spectral data in the free shear layer downstream of separation. Turbulence intensity profiles were acquired by amplifying and sampling the fluctuating portion of the hot-wire signal. A low-pass filter set nominally at 5000 Hz was used to remove the high-frequency noise associated with the amplifier. At each station, the spectral data were acquired at the predetermined point of maximum turbulence intensity at a sampling rate of 5000 Hz. The point of maximum turbulence intensity generally corresponded to the inflection point in the local velocity profile. Ensemble averaging was used to produce a single time history from which the energy spectral densities were calculated.

Experimental Results

During the data acquistion phase of this investigation, the separation bubble flowfield over the airfoil was surveyed for 12 different conditions. These particular conditions were chosen in order to isolate the effects of Reynolds number, angle of attack, and disturbance environment. The resulting experimental data were used to determine the magnitudes of the important separation bubble parameters (Fig. 2). These data provided detailed documentation of the behavior and structure of typical laminar separation bubbles. In addition, the data were analyzed and compared to existing separation bubble correlations. The measured parameters for each of the 12 cases are listed in Tables 2 and 3.

For each condition, the point locations defining the separation bubble were determined after a close examination of both the pressure and hot-wire anemometry data. The pressure data proved especially useful since the bubbles formed on the NACA 66_3-018 airfoil at angles of attack of 10 and 12 deg produced well-defined pressure "plateaus." A consistent point location for separation was determined by identifying the start of the constant-pressure region in the distribution and then correlating this location with the first appearance of an infinite slope at the wall in the velocity profiles. The point of free shear layer transition was taken as the downstream edge of the constant-pressure region. This location was confirmed by the corresponding hot-wire anemometry data, which indicated a large jump in the level of maximum turbulence intensity and a broadband energy spectrum downstream of this station.[2] The point of reattachment was taken as that point at which the pressure distribution exhibited a sharp decrease in the rate of pressure increase. This sometimes required interpolation between the pressure stations. Identifying the exact extent of the separation bubble was limited by the inability of the single-wire probe to determine the local flow direction.

The separation angle γ was determined using the hot-wire velocity profiles just downstream of separation. From these profiles, the heights of the recirculation region were plotted vs the surface arc length and a linear extrapolation technique

Table 2 Important flowfield parameters

Parameter \ Condition	$R_c = 140$K $\alpha = 12$ deg 0*FR*	$R_c = 160$K $\alpha = 12$ deg 0*FR*	$R_c = 200$K $\alpha = 12$ deg 0*FR*	$R_c = 50$K $\alpha = 12$ deg 1*FR*	$R_c = 80$K $\alpha = 10$ deg 1*FR*	$R_c = 80$K $\alpha = 12$ deg 1*FR*
l_B, S/C%	13.6	12.3	9.0	22.0	12.7	16.7
l_1, S/C%	7.1	6.4	4.8	12.9	8.3	9.2
l_2, S/C%	6.5	5.9	4.2	9.1	4.4	7.5
$(H_B)_T$, %C	0.54	0.46	0.29	1.13	0.54	0.80
H_T, %C	0.79	0.64	0.46	1.69	0.77	1.29
U_S, m/s	17.0	19.9	25.6	5.7	9.2	9.4
U_T, m/s	17.1	20.0	25.4	5.6	9.2	9.4
U_R, m/s	13.5	15.5	20.3	4.5	7.4	7.5
$(\delta_1)_S$, %C	0.16	0.18	0.14	0.25	0.23	0.24
$(\delta_1)_R$, %C	0.63	0.66	0.35	1.37	0.45	0.90
$(\delta_2)_S$, %C	0.040	0.034	0.036	0.059	0.059	0.050
$(\delta_2)_R$, %C	0.36	0.37	0.20	0.65	0.25	0.48
$(H_{12})_S$	4.09	4.66	3.88	4.16	3.90	4.48
$(H_{12})_R$	1.75	1.78	1.72	2.08	1.82	1.88

Parameter \ Condition	$R_c = 100$K $\alpha = 10$ deg 1*RF*	$R_c = 100$K $\alpha = 12$ deg 1*FR*	$R_c = 140$K $\alpha = 12$ deg 1*FR*	$R_c = 50$K $\alpha = 10$ deg 2*FR*	$R_c = 50$K $\alpha = 12$ deg 2*FR*	$R_c = 140$K $\alpha = 12$ deg 2*FR*
l_B, S/C%	10.2	14.2	10.3	15.5	18.8	9.0
l_1, S/C%	6.9	7.8	5.5	10.0	11.0	4.8
l_2, S/C%	3.3	6.4	4.8	5.5	7.8	4.2
$(H_B)_T$, %C	0.42	0.63	0.37	0.67	1.13	0.33
H_T, %C	0.67	0.82	0.63	0.86	1.39	0.54
U_S, m/s	11.7	12.0	17.3	5.7	5.8	17.9
U_T, m/s	11.7	12.1	17.2	5.7	5.8	17.9
U_R, m/s	9.5	9.5	13.5	4.6	4.6	14.0
$(\delta_1)_S$, %C	0.19	0.23	0.19	0.26	0.25	0.17
$(\delta_1)_R$, %C	0.41	0.75	0.44	0.81	1.34	0.41
$(\delta_2)_S$, %C	0.052	0.043	0.044	0.079	0.073	0.040
$(\delta_2)_R$, %C	0.23	0.39	0.26	0.35	0.60	0.23
$(H_{12})_S$	3.50	4.91	4.28	3.26	3.38	4.20
$(H_{12})_R$	1.75	1.94	1.71	2.30	2.25	1.75

Table 3 Important flowfield parameters

Parameter \ Condition	$R_c = 140$K $\alpha = 12$ deg 0*FR*	$R_c = 160$K $\alpha = 12$ deg 0*FR*	$R_c = 200$K $\alpha = 12$ deg 0*FR*	$R_c = 50$K $\alpha = 12$ deg 1*FR*	$R_c = 80$K $\alpha = 10$ deg 1*FR*	$R_c = 80$K $\alpha = 12$ deg 1*FR*
$(H_{32})_S$	1.49	1.57	1.51	1.52	1.53	1.54
$(H_{32})_R$	1.65	1.64	1.66	1.56	1.63	1.61
$Rl_B \times 10^{-4}$	3.71	3.85	3.76	2.05	1.88	2.42
$Rl_1 \times 10^{-4}$	1.95	2.01	2.03	1.20	1.23	1.34
$(R_S)_S \times 10^{-4}$	1.92	2.20	3.04	0.656	1.00	1.02
$(R_S)_T \times 10^{-4}$	3.87	4.21	5.06	1.86	2.23	2.36
$(R_{\delta 1})_S$	445.0	557.0	589.0	229.0	346.0	343.0
$(R_{\delta 2})_S$	109.0	105.0	150.0	55.0	87.0	72.0
α_T, deg	29.0	25.5	27.5	35.5	30.0	26.5
γ, deg	8.0	6.5	6.0	9.0	4.0	6.5
$(H_{12})_{S'}$	2.56	2.79	2.69	1.87	2.40	2.10
$(H_{32})_{S'}$	1.53	1.52	1.53	1.63	1.55	1.58

Parameter \ Condition	$R_c = 100$K $\alpha = 10$ deg 1*RF*	$R_c = 100$K $\alpha = 12$ deg 1*FR*	$R_c = 140$K $\alpha = 12$ deg 1*FR*	$R_c = 50$K $\alpha = 10$ deg 2*FR*	$R_c = 50$K $\alpha = 12$ deg 2*FR*	$R_c = 140$K $\alpha = 12$ deg 2*FR*
$(H_{32})_S$	1.51	1.48	1.50	1.50	1.53	1.50
$(H_{32})_R$	1.66	1.61	1.66	1.55	1.57	1.65
$Rl_B \times 10^{-4}$	1.86	2.64	2.80	1.40	1.73	2.54
$Rl_1 \times 10^{-4}$	1.26	1.44	1.48	0.903	1.01	1.37
$(R_S)_S \times 10^{-4}$	1.24	1.31	1.97	0.671	0.699	2.05
$(R_S)_T \times 10^{-4}$	2.50	2.75	3.46	1.57	1.71	3.42
$(R_{\delta 1})_S$	346.0	424.0	514.0	233.0	226.0	488.0
$(R_{\delta 2})_S$	96.0	79.0	119.0	71.0	67.0	113.0
α_T, deg	51.0	28.0	25.5	30.5	35.5	26.5
γ, deg	5.0	6.5	6.0	3.0	6.5	5.0
$(H_{12})_{S'}$	2.52	2.31	2.73	2.68	2.51	2.74
$(H_{32})_{S'}$	1.54	1.56	1.52	1.54	1.53	1.52

was employed to approximate the angular parameter. The resulting linear fits were generally valid over most of the laminar portion of the bubble. This procedure is illustrated in Fig. 4. The other angular parameter, the turbulence spreading angle α_T, was estimated using the geometric simplification shown in Fig. 5. In this procedure, the onset of bulence was assumed to take place at the point of maximum turbulence intensity at transition. From this point, the turbulence was assumed to spread linearly to the airfoil surface and the boundary-layer edge at reattachment.

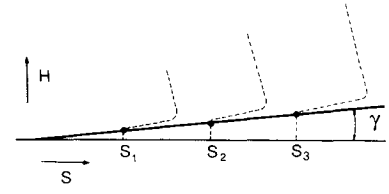

Fig. 4 Calculation technique for separation angle.

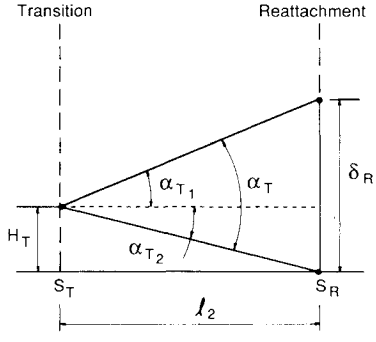

Fig. 5 Turbulent spreading angle.

Discussion of Results

Before each structural component of the bubble is described in detail, the overall dimensions and characteristics will be discussed. This discussion is aimed at revealing those variables significantly affecting the physical dimensions of the separation bubble. From this information, many of the important trends exhibited by the separation bubble parameters will become evident.

General Separation Bubble Characteristics

As shown in Fig. 6, the chord Reynolds number has an important effect on the laminar separation bubble. This figure shows the effects of Reynolds number for the three different tunnel configurations (varying levels of freestream disturbances). As expected, the length of the separation bubble increases as the chord Reynolds number is decreased. With one flow restrictor in place, the bubble more than doubles in length as the chord Reynolds number is decreased from $R_c = 140{,}000$ to 50,000. The other flow restrictor cases exhibit the same trend with Reynolds number, although the magnitudes of l_B are shifted. This is made evident by the dotted line connecting the three cases at $R_c = 140{,}000$. The shift in magnitude of l_B indicates that bubble length is also a function of the disturbance environment. Although the disturbances increased slightly as the chord Reynolds number (tunnel speed) was increased, the Reynolds number effect appears to predominate.[2]

Through use of the various tunnel configurations, it was possible to isolate the disturbance environment. These effects are revealed in the pressure distributions shown in Fig. 7. As the disturbance level is increased, the bubble is reduced in length and the suction peak grows in absolute magnitude. This well-known phenomenon so closely resembles the effects obtained by increasing the chord Reynolds number that the two are often equated. This has given rise to the use of

"effective" Reynolds numbers when dealing with various disturbance environments or when discussing the effects of different types of surface roughness.

Along with chord Reynolds number and freestream disturbances, the separation bubble is also affected by changes in angle of attack. These effects are summarized in Fig. 8. As the angle of attack is increased from 8 to 10 deg, the point of laminar separation moves forward from approximately 3.7 to 2.8% X/C, but there is no significant change in the length of the bubble. At an angle of 12 deg, the bubble has again moved forward, but has now increased in length. The forward movement of separation with increasing angle of attack is due primarily to the more severe adverse pressure gradient occurring at higher incidences. At a given angle of attack, the separation point remains essentially unchanged over the entire range of Reynolds numbers.

In addition to the overall length, the thickness of the separation bubble is a parameter significantly affected by the various testing conditions. For the sake of comparison, the height of the recirculation region at transition $(H_B)_T$ was determined from each set of velocity profiles.[2] These thicknesses are plotted vs chord Reynolds number in Fig. 9. This figure indicates that a sharp reduction in bubble thickness occurs as the chord Reynolds number is increased. The bubble at $R_c = 50{,}000$ is almost three times thicker at transition than the corresponding bubble at $R_c = 140{,}000$. This would seem to imply that the bubble thickness is closely related to the total bubble length. This almost linear relationship is plotted in Fig. 10. Although only limited number of points are available, the values in Table 2 also indicate that the bubble thickness increases as the angle of attack is increased. This phenomenon was confirmed by the flow visualization data.[2]

In general, the pressure distribution upstream of the separation bubble appears to be highly dependent not only on the angle of attack, but also on the chord Reynolds number and the disturbance environment. As the chord Reynolds number or disturbance environment are increased, the bubble decreases in length and thickness, resulting in a less "disturbed" pressure distribution with a higher suction peak. This increased sensitivity in the upstream pressure distribution appears to be an important factor in low Reynolds number airfoil aerodynamics. Downstream of the bubble, however, the pressure distribution is less affected by the testing conditions.

Laminar Portion of Bubble

The location of laminar separation on an airfoil at incidence has been studied in great detail. Both experimental and theoretical techniques have been employed to determine representative values of the boundary-layer parameters at this location.[5-7] The most commonly used parameter is the shape factor $H_{12} = \delta_1/\delta_2$. Unfortunately, this factor increases sharply near separation due to the rapid growth in displacement thickness δ_1 in the region of separated flow. This large gradient region coupled with the small uncertainty in the location of separation make H_{12} a somewhat unreliable parameter. These conditions also account for the relatively large range of values listed in Table 2.

Because it remains essentially invariant throughout regions of separated flow, the second shape factor $H_{32} = \delta_3/\delta_2$ provides a much better comparison. The average value of H_{32} at separation for the complete set of data was 1.515 and the associated sample standard deviation was 0.025. This average value is exactly equal to that used by Eppler and Somers[7] in their airfoil analysis code. This constant value could be useful in the development of a separation bubble model since it relates the two thicknesses at separation.

One of the most important parameters at separation is the local Reynolds number based on the external velocity and the momentum thickness. Many of the important structural parameters of the bubble have been shown to be directly

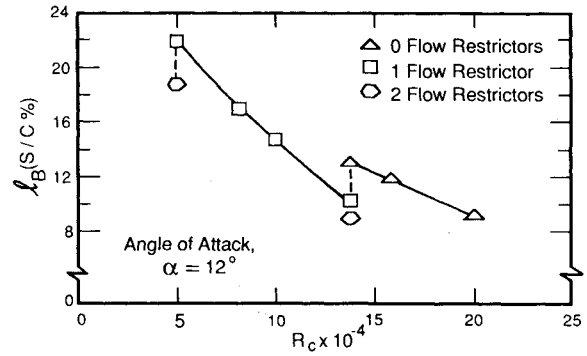

Fig. 6 Total bubble length vs Reynolds number.

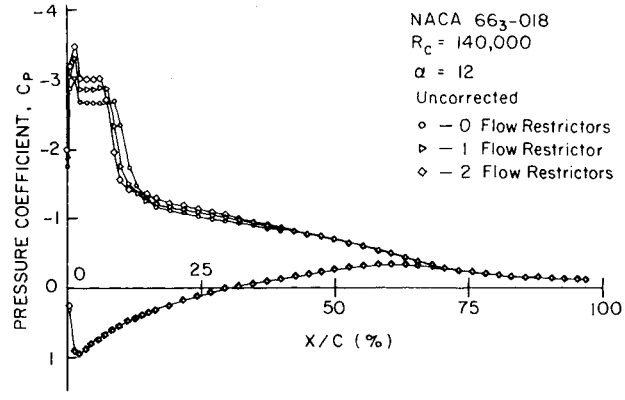

Fig. 7 Effect of freestream disturbance level on pressure distribution ($R_c = 140{,}000$, $\alpha = 12$ deg).

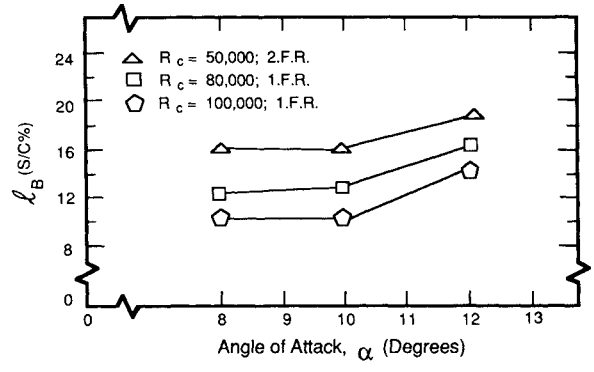

Fig. 8 Total bubble length vs angle of attack.

dependent on the magnitude of R_{δ_2} at separation.[8,9] As expected, the experimentally determined values listed in Table 3 indicate that this parameter is a function of the chord Reynolds number and the external velocity distribution up to separation.[5] The dependency is such that the value of R_{δ_2} at separation generally increases, within the uncertainty of the data, as the chord Reynolds number is increased. As the angle of attack is increased from 10 to 12 deg, R_{δ_2} at separation decreases. This is primarily due to the forward movement of the bubble, which causes a decrease in the value of δ_2 at separation.

Separation Angle

Downstream of separation, the geometry of the bubble is dictated by the angle at which the separation streamline leaves the wall. In this investigation, the separation angle γ was determined using the extrapolation procedure described earlier (Fig. 4). As Table 3 indicates, the values of this parameter correlate well with the trends in bubble thickness. As the chord Reynolds number is increased, the separation

angle decreases and the bubble is reduced in thickness. The separation angle increases as the angle of attack is increased, a trend consistent with the growth in bubble thickness described earlier. As one might expect, increases in the disturbance levels have the same effect on γ as increases in the chord Reynolds number.

Because of its importance in dictating the structure of the bubble downstream of separation, the separation angle is often a parameter of interest in semiempirical models. Since traditional laminar boundary-layer calculations are valid only up to separation, it might be desirable to relate the conditions at separation of the resulting value of γ. Such a relationship was suggested by Dobbinga et al.,[9] who used the value of R_{δ_2} at separation to incorporate the various separation conditions. These investigators postulated that the tangent of γ was inversely proportional to the value of R_{δ_2} at separation. Through their experiments, a range (15-20) of the proportionality constant B was determined. They also suggested that B should be a constant for a given model at a given angle of attack.

A plot of the tangent of γ vs R_{δ_2} at separation for the present data is shown in Fig. 11. In general, there is very little deviation in the value of the separation angle for the 12 deg angle of attack cases. Over the range of R_{δ_2}, γ varies only between 5-9 deg. As the figure indicates, only two of the measured cases fall within the range suggested by Dobbinga et al.[9] These points represent the high chord Reynolds number ($R_c = 140{,}000$ and 200,000) and the low freestream turbulence intensity ($0FR$) conditions. Since these data should correspond to a single value of B according to Dobbinga et al., the applicability of the suggested functional relationship appears to be questionable.

One of the assumptions made by Dobbinga et al.[9] in developing the proposed relation was that the variations in chord Reynolds number R_c have little or no effect on the nondimensional pressure distribution around a given body at a given angle of attack. Although this is probably a valid assumption at higher Reynolds numbers ($R_c = 1 \times 10^6$ and above) where very small separation bubbles form, this assumption does not appear to hold at lower Reynolds numbers. It should also be noted that the data compiled by these researchers were obtained primarily on flat plates and circular cylinders where the separation was often induced by external means. Perhaps a direct extension to natural separation on an airfoil cannot be made easily. It appears from the present data that this correlation must be made sensitive to variations in the pressure distribution before consistent and reliable results can be achieved at low Reynolds numbers.

Length of Laminar Layer and Prediction of Transition

The most crucial point in calculating the flow through a laminar separation bubble involves accurately predicting the point of transition. It is at this point that the governing equations are often "switched" from the laminar to the turbulent form. In most calculation schemes, empirically derived relations are used to determine the location of the transition. In general, these corrections relate the conditions at separation to some parameter indicative of the transition. Several of the correlations developed[9,10] involve the length of the laminar layer l_1. Another approach[11] involves the use of the height of the zero-velocity streamline at transition. Because much of the data used in formulating these relations were obtained at higher chord Reynolds numbers (on the order of 1×10^6), the applicability to lower Reynolds number cases must be determined.

In general, the length of the laminar portion of the bubble depends on the disturbance amplification process occurring in the free shear layer. This process is directly affected by the chord Reynolds number, angle of attack, and disturbance environment. The trends resulting from these dependencies can be seen in Table 2. As the chord Reynolds number is in-

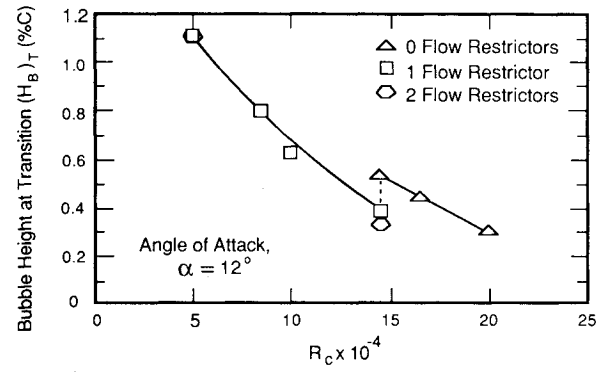

Fig. 9 Bubble height at transition vs chord Reynolds number.

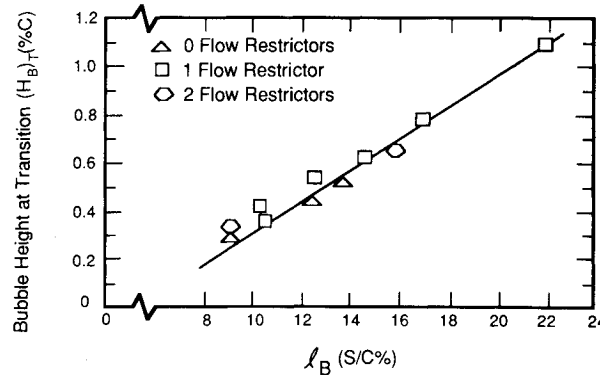

Fig. 10 Bubble height at transition vs total bubble length.

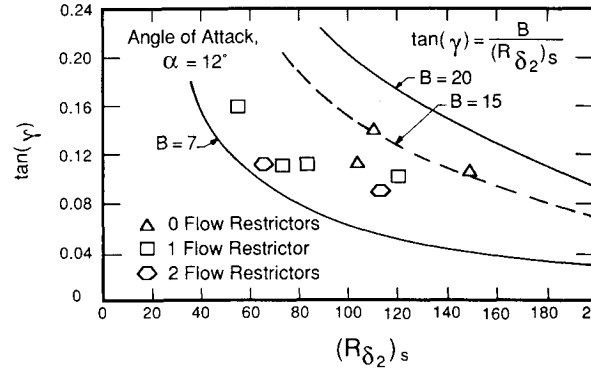

Fig. 11 Tangent of separation angle vs Reynolds number based on momentum thickness at separation (from Ref. 9).

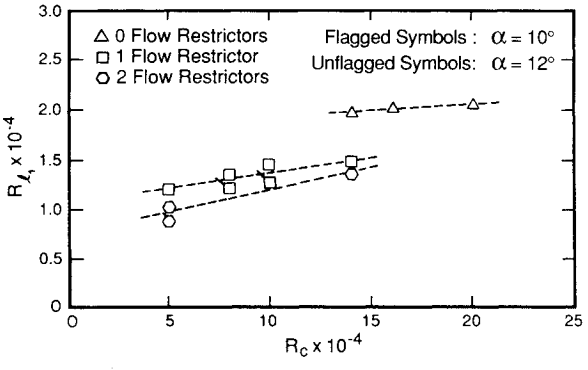

Fig. 12 Reynolds number based on laminar bubble length vs chord Reynolds number.

creased, l_1 decreases due to earlier transition. As the angle of attack is increased from 10 to 12 deg, the magnitude of l_1 increases, but the laminar length becomes a significantly smaller percentage of the entire bubble. This implies that the angle-of-attack change has a more pronounced effect on the length of the turbulent portion of the bubble.

A commonly used parameter involving the laminar length l_1 is the Reynolds number based on this length and the external velocity at separation. In early separation bubble studies, this parameter was believed to be universally constant. Although later studies showed that this assumption was at best a first-order approximation, some important correlations have been developed using this same basic theme. The values of R_{l_1} calculated from the present data are plotted in Fig. 12. The highest chord Reynolds number cases ($R_c = 140{,}000$–$200{,}000$) indicate a relatively constant value of R_{l_1} of approximately 20,000, while the lower chord Reynolds number cases exhibit a more noticeable increase with increasing R_c. A definite disturbance environment dependency is indicated by the multiple values of R_{l_1} measured at a constant chord Reynolds number of 140,000. R_{l_1} also increases slightly with the increasing angle of attack as both the separation velocity and length parameter l_1 experience increases in magnitude.

Although realizing the potential limitations involved, Horton[8] attempted to correlate the momentum thickness

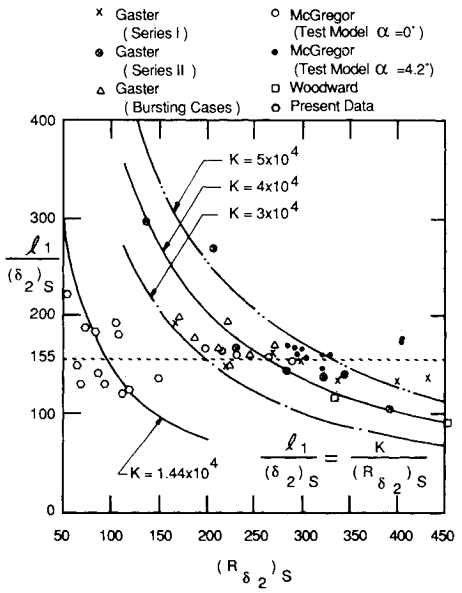

Fig. 13 Nondimensional laminar length vs momentum thickness Reynolds number at separation (from Ref. 8).

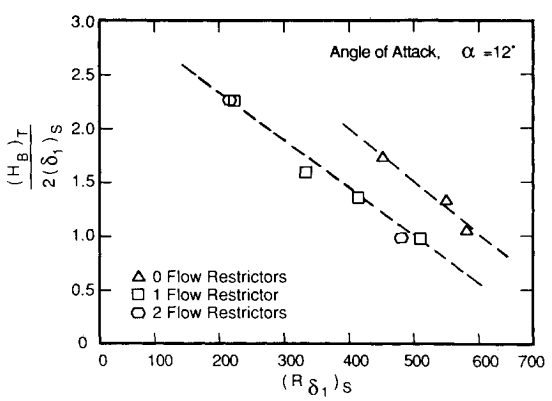

Fig. 14 Approximate height of zero velocity streamline at transition vs displacement thickness Reynolds number at separation.

Reynolds number at separation to the resulting nondimensional laminar length. He tentatively postulated that $l_1(\delta_2)_S$ was inversely proportional to R_{δ_2} at separation. This functional form merely restated the existing assumption that R_{l_1} should be universally constant. A plot of the attempted correlation and some existing experimental data are shown in Fig. 13. The present data are also included in this plot in order to identify any possible functional relationship. A value of the proportionality constant K for the present data was determined by calculating a mean value of R_{l_1} for the entire range of the testing conditions. This calculated value was then used to construct a curve following the functional form suggested by Horton.

The present data plotted in Fig. 13 appear to follow no obvious trend. Although a few points fall close to the suggested curve, the proposed functional form does not seem to hold, as previously noted, for the low chord Reynolds number data. The scattering of the data around a mean value of $l_1/(\delta_2)_S$ of 155, however, is consistent with the data used by Horton. In fact, a constant value for the nondimensional laminar length appears to be the best representation over the entire range of local Reynolds numbers. In order to truly identify a functional relationship, if one even exists, additional data and analysis are required.

A somewhat different correlation for predicting transition onset in a separation bubble has been proposed by Crimi and Reeves.[11] They formulated an analogy between transition in the separated shear layer and boundary-layer tripping caused by an element of surface roughness. This analogy eventually led to the development of a functional relationship between the displacement thickness Reynolds number at separation and the nondimensional height of the zero velocity curve at transition. This relationship, which was determined from airfoil data, shows the thickness to be inversely proportional to the square of R_{δ_1} at separation. In order to attempt such a correlation for the present data, the height of the zero velocity point at transition was approximated by one-half of the total bubble thickness at this location.[2] The resulting data are shown in Fig. 14 for the 12 deg angle-of-attack cases. In general, a linear variation is indicated along with a well-defined dependency on the disturbance environment. The implications of this unexpected trend are not fully understood and an exact explanation for this behavior cannot be provided at present. Perhaps the relatively invarient character of the separation angle, which partially dictates bubble thickness, is a cause of this phenomenon.

Turbulent Portion of Bubble

As discussed thus far, the transition from laminar to turbulent flow in the free shear layer has been assumed to occur

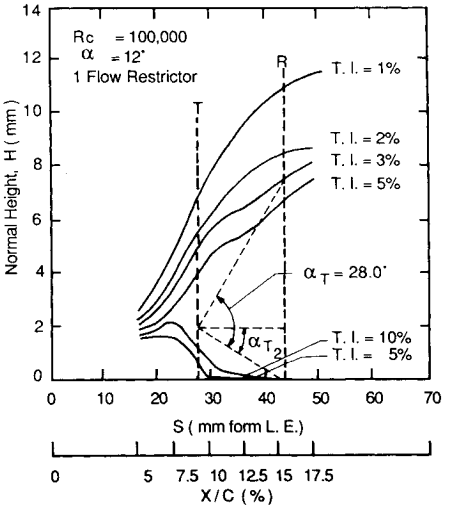

Fig. 15 Lines of constant turbulence intensity from transition to reattachment.

over a very short distance. This allowed a point location to be assigned to this phenomenon. In general, however, a finite transition region is expected. Because of the accelerated transition process in the free shear layer, the transitional region of the separation bubble is expected to be shorter than might exist in the case of an attached boundary layer. In fact, an instantaneous transition model has been shown in some cases to give surprisingly good results.[10] Thus, although the concept of instantaneous transition may not be physically acceptable, this region appears to be small enough to allow a point location to be used in the modeling process.

The height of transition H_T is an important parameter in the simplified bubble model shown in Fig. 2. From the present data, this parameter is defined as the height of the maximum turbulence intensity point at transition. This point generally corresponds to the inflection point in the transitional velocity profile and is usually located at or near the vertical center of the free shear layer. As expected, the values of H_T listed in Table 2 show that this parameter is dictated by the bubble thickness. From a geometric standpoint, H_T is a function of l_1, γ, and the shear layer growth from separation to transition. As a result, it is not surprising that this parameter decreases with increasing chord Reynolds number and increases with increasing angle of attack.

The turbulent spreading angle α_T shown in Fig. 2 is approximated using the geometrically simplified procedure described earlier. This scheme assumes that the turbulence spreads linearly from the point H_T to the boundary-layer edge and airfoil surface at reattachment. In an attempt to verify this linear growth, lines of constant turbulence intensity have been plotted for a representative case. In essence, these "isoturbulence" lines (shown in Fig. 15) outline the region of increased intensity associated with turbulent free shear layer. As expected, a large vertical growth in the region occurs near the point of transition. This figure, which also includes the lines forming the defined spreading angle, indicates that the growth is approximately linear except for the area close to reattachment. The lower two curves reveal that the turbulence spreads to the wall more rapidly than the proposed angle would indicate. This is confirmed by the turbulence intensity profiles, which show relatively high levels of intensity near the wall just downstream of transition.[2] Figure 15 also shows the asymmetric spread of turbulence about the point H_T. In general, the lower angle α_{T2} is approximately 30% of the total spreading angle for the present data.

The values of α_T calculated from the present data are plotted in Fig. 16. This plot shows the relatively inconsistent nature of this parameter. As one might expect, the turbulent spreading angle generally decreases in magnitude with increasing chord Reynolds number, but this trend is not consistent. Since the three parameters defining this angle (δ_R,H_T,l_2) are each affected by changes in the testing conditions, it is difficult to predict the behavior of α_T. The lack of consistent behavior is most likely due to the extreme sensitivity of this angle to the length dimensions used in the calculation process. The boundary-layer thickness at reattachment, for example, significantly affects the magnitude of α_T, yet it is a difficult height to determine consistently. This problem, along with the very short turbulent free shear layers that occur at the lower angles of attack, resulted in the unusually large calculated value of α_T (51 deg) for the $R_c = 100{,}000$, $\alpha = 10$ deg, single-flow restrictor case. Although this parameter may have some validity, the difficulty in estimating its magnitude severely hampers its usefulness. Perhaps plots similar to Fig. 17 can be used to define a similar but more consistent spreading parameter.

From the present data, it appears that the length of the turbulent shear layer l_2 is primarily dependent on the transition height H_T and the amount of pressure recovery from transition to reattachment. As indicated in Table 2, the most significant change in l_2 occurs as the angle of attack is increased from 10 to 12 deg, which coincides with a large growth in the bubble thickness. This is partially due to the fact that, as the bubble increases in thickness, more entrainment is required to eliminate the reverse flow region near the wall. This generally results in a longer turbulent shear layer. Another important factor is the level of pressure recovery occurring over the turbulent portion of the bubble. In fact, some consistency in the amount of pressure increase over the turbulent portion of the bubble has been discovered. This fact implies that parameters similar to those used to predict the onset of bubble bursting may be useful in the modeling process.[8]

Turbulent Reattachment

Using a criterion analogous to the laminar and turbulent separation criteria of Thwaites and Buri, Horton was able to predict the location of turbulent reattachment.[8] Although his primary interest was in the bursting of laminar separation bubbles, his results can be used to aid in the calculation of the separation bubble geometry. Using data obtained by Mueller and Tani, Horton was able to provide evidence for the universality of the reattachment velocity profile. The shape factors $(H_{12})_R$ and $(H_{32})_R$ determined from this profile were approximately 3.5 and 1.5, respectively. As already noted H_{12} is a difficult parameter to use for comparison because of the large variations in the vicinity of the bubble. The $(H_{12})_R$ values calculated from the present data, however, never exceed 2.3.

As indicated in Table 3, the reattachment value of H_{32} suggested by Horton is somewhat lower than the values calculated from the present data. The present mean value of 1.62 (sample standard deviation = 0.041) is more consistent with Eppler and Somer's[7] suggestion that the laminar separation bubble should extend at least to the point where $H_{32} = 1.58$. In general, further investigation into the exact location of the reattachment and the corresponding condi-

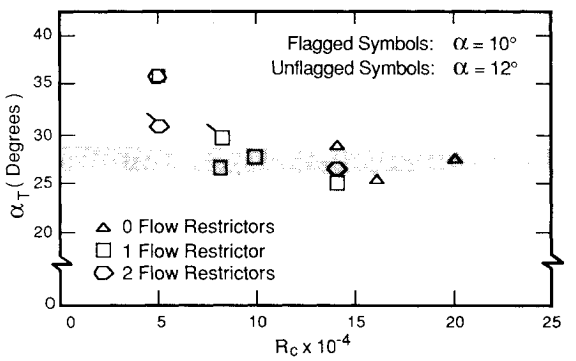

Fig. 16 Turbulent spreading angle vs chord Reynolds number.

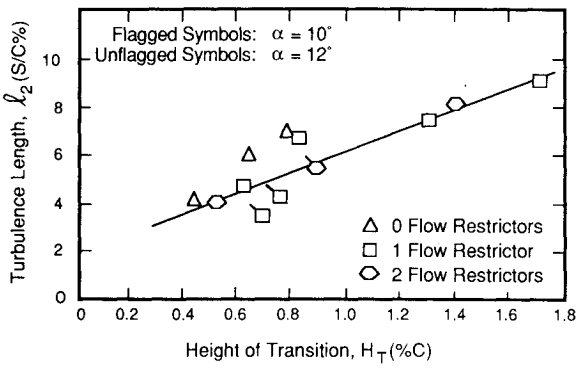

Fig. 17 Turbulent bubble length vs height of transition.

tions needs to be performed before the assumption of a universal profile can be verified.

Conclusions

From a behavioral standpoint, the laminar separation bubble that forms on the NACA 66_3-018 airfoil decreases in length and thickness as the chord Reynolds number is increased. As the angle of attack is increased from 10 to 12 deg, the bubble increases in both length and thickness. The effects of the disturbance environment are very similar to those produced by increases in the chord Reynolds number. In general, an almost linear relationship exists between the bubble thickness and the total bubble length.

Although a potentially useful parameter, the separation angle is a difficult quantity to measure. The values of this angle derived from the present data range 5–9 deg in magnitude. This represents a surprisingly small range of values. The separation angles measured in the highest chord Reynolds number cases fall close to the correlation developed by Dobbinga et al.[9] Although this correlation indicates that the present data should follow a single relationship, a range of correlation constants is needed to encompass the full set of data. Thus, it appears that this correlation must be modified in order to be applicable to low chord Reynolds number data.

In terms of predicting the point of free shear layer transition, no conclusive agreement is found between the present data and the existing correlations. The applicability of the empirical relationships attempted by Horton,[8] for example, seems to be questionable. Some consistency is evident, however, in the magnitudes of the nondimensional laminar lengths. The inconsistencies with the established correlations are due primarily to the strong dependency of the low Reynolds numbers pressure distributions on the chord Reynolds number and the disturbance environment. These effects must be included in any correlation that is to be applied to the low Reynolds number flight regime.

Like the separation angle, the turbulent spreading angle is a difficult parameter to determine. In this investigation, this parameter proved to be extremely sensitive to the length dimensions used in the calculation process. Because of the inconsistent nature of this angle, no conclusive results could be determined. Further studies must be conducted in order to determine a more representative and consistent turbulent spreading parameter.

Although the existence of a universal reattachment velocity profile has been suggested by some investigators, the boundary-layer parameters at reattachment from the present data exhibit a significant amount of scatter. Additional data near the location of flow reattachment are needed to sufficiently evaluate this claim.

Acknowledgment

This research was supported by NASA Langley Research Center under Grant NSG-1419 and the Department of Aerospace and Mechanical Engineering, University of Notre Dame.

References

[1]Robers, W. B., "Calculation of Laminar Separation Bubbles and Their Effect on Airfoil Performance," *AIAA Journal*, Vol. 18, Jan. 1980, pp. 25–30.

[2]O'Meara, M. M., "An Experimental Investigation of the Separation Bubble Flow Field Over an Airfoil at Low Reynolds Numbers," M.S. Thesis, University of Notre Dame, Notre Dame, IN, 1985.

[3]Mueller, T. J., Pohlen, L. J., Conigliaro, P. E., and Jansen, B. J. Jr., "The Influence of Freestream Disturbances on Low Reynolds Number Airfoil Experiments," *Experiments in Fluids*, Vol. 1, Springer-Verlag, Berlin, 1983, pp. 3–14.

[4]Marchman, J. F. III, Sumantran, V., and Schaefer, C. G., "Acoustic and Turbulence Influences on Stall Hysteresis," AIAA Paper 86-170, Jan. 1986.

[5]Schlichting, H., *Boundary-Layer Theory*, (7th ed.), McGraw-Hill, New York, 1979.

[6]Tani, I., "Low Speed Flows Involving Bubble Separations," *Progress in Aeronautical Sciences*, Vol. 5, Macmillian, New York, 1964, pp. 70–103.

[7]Eppler, R. and Somers, D. M., "A Computer Program for the Design and Analysis of Low-Speed Airfoils," NASA TM 80210, Aug. 1980.

[8]Horton, H. P., "Laminar Separation Bubbles in Two and Three Dimensional Incompressible Flow," Ph.D. Thesis, University of London, London, 1968.

[9]Dobbinga, E., van Ingen, J. L., Kooi, J. W., "Some Research on Two-Dimensional Laminar Separation Bubbles," AGARD CP-102, 1972, Paper 2.

[10]Kwon, O. K. and Pletcher, R. H., "Prediction of Incompressible Separated Boundary Layers Including Viscous-Inviscid Interaction," *Transactions of ASME*, Vol. 101, 1979, pp. 466–472.

[11]Crimi, P. and Reeves, B. L., "Analysis of Leading-Edge Separation Bubbles on Airfoils," *AIAA Journal*, Vol. 14, Nov. 1976, pp. 1548–1555.